Dynamic ordering of driven spherocylinders in a nonequilibrium suspension of small colloidal spheres

Anton Lüders, Ullrich Siems,* and Peter Nielaba
Department of Physics, University of Konstanz, 78457 Konstanz, Germany

(Received 1 September 2018; published 1 February 2019)

The ordering effects of driven spherocylinder-shaped rods in a colloidal suspension of small spheres confined to a two-dimensional channel geometry are observed via Brownian dynamics simulations without hydrodynamics. To describe the ordering, an order parameter and an expression for a potential of mean force of an equivalent equilibrium system are defined and analyzed. By varying the application point of the external force along the rods and thus the resulting lever, a transition from a preferred orientation parallel to the direction of the force to a preferred orientation perpendicular to the direction of the force was observed. It is shown that this effect can only be found if the spheres and multiple rods are present. Furthermore, a dependency of the order parameter on the absolute value of the force was discovered. The analysis of the potential of mean force further indicates a transition between two different phases of mean orientation. An observation of the flow equilibrium mean velocity in channel direction led to a *s*-shaped progression regarding the lever dependency, also marking a transition between two states linked to the mean orientation of the rods. A finite size analysis was conducted. Its results indicate that the transition between the two orientation states is a general phenomenon of the observed rod-sphere mixture.

DOI: 10.1103/PhysRevE.99.022601

I. INTRODUCTION

Nonequilibrium systems are of high interest for modern research. In comparison with the well known classical equilibrium physics, many phenomena are completely new or unknown. Therefore, out-of-equilibrium colloidal model systems are a venue to analyze and find different dynamical phenomena [1–8]. Moreover, colloidal studies regarding restricted microchannels [9–13] further the understanding of complex systems like atomic wires [14,15] and laboratory-on-a-chip devices [16,17].

Binary colloid systems of differently driven two- or three-dimensional particles are very suitable for extensive nonequilibrium studies and many detailed observations of such systems based on spherical particles [18–22] exist. An important phenomenon of these models is the formation of lanes, which corresponds to a common observation on pedestrians moving in opposite directions [23–25].

Due to the symmetry of the spherical particles, the orientation is not a relevant state variable in these systems. This is changed by replacing multiple spherical particles by rods. These so formed rod-sphere mixtures provide interesting results in equilibrium and nonequilibrium simulations [26–28] and experiments [29]. A recent study has also shown that different types of complex large particles in a bath of small driven spheres show ordering in stripes and clusters [30].

By driving the rod-shaped particles through the spheres by means of a constant force acting on their center of mass, the typical lane formation and an additional aligning effect are found in simulations [31]. This indicates exciting ordering effects of driven rods in a nonequilibrium bath of spheres.

Due to the shape of the rods, a degree of freedom is given by the position of the point of force application in relation to their particular centers. An off-center force results in a force moving the centers of the rods and an additional torque, consequently the orientation of the rods is affected. So the preferred orientation of the rod should exhibit a dependency on the resulting lever arm.

In this work the main objective is to study the ordering of driven rods surrounded by additional spheres in a liquid bath by two-dimensional Brownian dynamics simulations without hydrodynamic interactions. The lever dependency of the preferred orientation is investigated, so that statements about the different ordering effects are possible. The definition of an order parameter and the analysis of probability distributions, potentials of mean force, and the flow equilibrium mean velocities in channel direction lead to a better understanding of the resulting rod orientation.

Surprising ordering mechanisms are found regarding the rod-sphere mixture: A force applied to one end of the rods results in an ordering parallel to the direction of the driving force. In contrast to this process, the rods order differently for a force applied to their centers. A force applied to the centers of the rods leads to a preferred orientation perpendicular to the direction of the force. All observed quantities indicate a transition between these two states.

This paper is structured as follows: In Sec. II the model and the numerical methods are discussed and the order parameter as well as the potential of mean force for a corresponding equilibrium system are defined. Following that, the results are presented in Sec. III, whereby the nonequilibrium state of

*ullrich.siems@uni-konstanz.de

FIG. 1. Sketch of a spherocylinder in two dimensions. It consists of a rectangle and two half circles. A spherocylinder is described by its length L, the line segment l, and its diameter σ_{sc}.

the spheres, the mean orientation of the rods, the influence of the different parts of the simulation setup, the resulting effective potentials, and the flow equilibrium mean velocity are discussed separately. Furthermore, a finite size analysis is presented in this section. This work is concluded with a summary in Sec. IV.

II. MODEL AND METHODS

Brownian dynamics (BD) simulations of a two-dimensional rod-sphere mixture in a channel geometry confined by soft walls perpendicular to the y direction and periodic boundary conditions in the x direction were performed. The particles are suspended in a liquid and hydrodynamic interactions are neglected.

A. Colloid modeling and BD method

The geometrical form of the rods is given by a spherocylinder. In the two-dimensional case, this special form consists of a rectangular middle section with a half circle at each end, as shown in Fig. 1.

The spherocylinder is defined by two parameters: its width or diameter σ_{sc} and its aspect ratio $q = L/\sigma_{sc}$, where L is the length of the spherocylinder. In the simulations a spherocylinder is represented by a line segment of length $l = L - \sigma_{sc}$ in its center. The surface of this geometrical form is defined by all points that have a distance of $\sigma_{sc}/2$ to this line segment.

The motion of the colloidal particles is assumed to be describable in overdamped approximation so that the inertial terms of the equations of motion are negligible. Thus, the masses of the spheres and the spherocylinders do not appear explicitly in the associated relations. The resulting equation of motion of a sphere in a fluid is given by the overdamped Langevin equation

$$\mathrm{v}(t) = \frac{D_\mathrm{s}}{k_B T}(\mathrm{F}(t) + \delta\mathrm{F}(t)), \tag{1}$$

where the velocity of a particle is determined by the instantaneous force F based on the sum of external forces and interaction forces and by the fluctuation force δF which is modeled by an independent, Gaussian distributed white noise. The constant of proportionality is composed of the diffusion coefficient of the spheres D_s, the Boltzmann constant k_B, and the temperature T. The position $\mathrm{r}_i(t)$ of the ith sphere was updated according to the Euler-Maruyama method. The new position after a time step Δt can be calculated with [32]

$$\mathrm{r}_i(t + \Delta t) = \mathrm{r}_i(t) + \frac{D_\mathrm{s}}{k_B T}\mathrm{F}_i(t)\Delta t + \sqrt{2D_\mathrm{s}\Delta t}\mathrm{R}, \tag{2}$$

where $\mathrm{F}_i(t)$ is the force acting on the ith particle and R is a vector with Gaussian random numbers characterized by vanishing mean $\langle R_i\rangle = 0$ and variance unity $\langle R_i^2\rangle = 1$, which we will call random numbers with standard normal distribution. In this study the diffusion coefficients themselves are used as fixed parameters. Hence, the variance of the fluctuation of the Brownian dynamics depends only on the used diffusion coefficient and Δt.

By means of the integrator (2), the movements of the centers of the spheres are completely described. To implement the Brownian motion of the rods, the orientation dependent diffusion of a spherocylindric colloid has to be taken into account. The implementation of the Brownian dynamics algorithm for the spherocylinders is based on the description in Ref. [33]. Therefore the motion of the center of a rod has to be split within a moving coordinate system in components parallel and perpendicular to the direction of the corresponding rod. Thereby, the rod direction can be represented with a unit vector $\hat{\mathrm{e}}$ parallel to the line segment of the structure. Then, the diffusion coefficients $D^\parallel$ and $D^\perp$ for these components are relevant. The position of the ith rod with the orientation $\hat{\mathrm{e}}_i$ can be split into

$$\mathrm{r}_i^\parallel(t) = (\hat{\mathrm{e}}_i(t)\cdot\mathrm{r}_i(t))\hat{\mathrm{e}}_i(t), \tag{3}$$

$$\mathrm{r}_i^\perp(t) = \mathrm{r}_i(t) - \mathrm{r}_i^\parallel(t). \tag{4}$$

The corresponding components of the force are given by

$$\mathrm{F}_i^\parallel(t) = (\hat{\mathrm{e}}_i(t)\cdot\mathrm{F}_i(t))\hat{\mathrm{e}}_i(t), \tag{5}$$

$$\mathrm{F}_i^\perp(t) = \mathrm{F}_i(t) - \mathrm{F}_i^\parallel(t). \tag{6}$$

To calculate the movement of the rods in three dimensions, the equations in Ref. [33] can be used as the numerical integrators. Variations of these equations for two dimensions are

$$\mathrm{r}_i^\parallel(t+\Delta t) = \mathrm{r}_i^\parallel(t) + \frac{D^\parallel}{k_B T}\mathrm{F}_i^\parallel(t)\Delta t + \sqrt{2D^\parallel\Delta t}R_1\hat{\mathrm{e}}_i(t), \tag{7}$$

$$\mathrm{r}_i^\perp(t+\Delta t) = \mathrm{r}_i^\perp(t) + \frac{D^\perp}{k_B T}\mathrm{F}_i^\perp(t)\Delta t + \sqrt{2D^\perp\Delta t}R_2\hat{\mathrm{e}}_i^\perp(t), \tag{8}$$

where R_k are random numbers with standard normal distribution and $\hat{\mathrm{e}}_i^\perp = (-e_y, e_x)^T$ is the unit vector perpendicular to the orientation vector $\hat{\mathrm{e}}_i = (e_x, e_y)^T$ of the ith rod.

The rotational Brownian motion of the two-dimensional rods in the overdamped limit is modeled by

$$\dot{\hat{\mathrm{e}}}(t) = \frac{D^r}{k_B T}[M(t) + \delta M(t)]\hat{\mathrm{e}}^\perp(t), \tag{9}$$

where D^r is the rotational diffusion coefficient, M is an additional scalar torque, and δM is a stochastic torque with analogous properties as the components of δF. The numerical implementation of the rotational movement is given by the equation in Ref. [33] adjusted for two dimensions. Thus, the time evolution of the unit vector parallel to the line segment of the ith rod can be computed by

$$\hat{\mathrm{e}}_i(t+\Delta t) = \hat{\mathrm{e}}_i(t) + \frac{D^r}{k_B T}M_i(t)\hat{\mathrm{e}}_i^\perp(t)\Delta t + \sqrt{2D^r\Delta t}R_3\hat{\mathrm{e}}_i^\perp(t). \tag{10}$$

It should be noted that $\hat{e}_i(t + \Delta t)$ has to be renormalized after each step. The diffusion coefficients for the translation and the rotation of the rods can, for example, be calculated by means of the equations in Ref. [33], which are based on the work of Ref. [34].

In our study, a model system is observed for which the diameter of the spherocylinders σ_{sc} is chosen as $\sigma_{sc} = 5\sigma_s$ and the aspect ratio is $q = 3$, where σ_s is the diameter of the spheres. For the diffusion constants of the rods $D^{\parallel} = 2.41 \times 10^{-2} D_s$, $D^{\perp} = 2.03 \times 10^{-2} D_s$, and $D^r = 3.93 \times 10^{-4} D_s/\sigma_s^2$ are used. With this parameter combination, the rods are still significantly bigger than the spheres, but the time scale of the diffusive rod movement is not too large in comparison with the simulation time and the characteristic time scale of the sphere diffusion. The set of diffusion coefficients used in this model system differs from the results of the related equations in Ref. [33].

By using these Brownian dynamics integrators, the system of spheres and spherocylinders corresponds to a binary colloid mixture in an external bath given by a liquid. Thereby, the effects of the bath on the particles are inherently contained in the Brownian dynamics algorithm by the friction forces and the stochastic terms of the integrators. The smaller spheres act like an additional bath for the observed spherocylinders. Thus, in the following the sphere system is often called a bath of spheres. The overdamped approximation of the particle motion is always handled in regard to the inherent bath of the Brownian dynamics.

B. Interactions and external drive

The interactions between the different parts of the observed system are solely repulsive. This is implemented as a soft repulsion by means of the Weeks-Chandler-Andersen potential [35]. The Weeks-Chandler-Andersen pair interaction is given by

$$V(\Delta r) = \begin{cases} 4\varepsilon\left[\left(\frac{\sigma}{\Delta r}\right)^{12} - \left(\frac{\sigma}{\Delta r}\right)^{6}\right] + \varepsilon, & \Delta r \leqslant 2^{1/6}\sigma, \\ 0, & \Delta r > 2^{1/6}\sigma, \end{cases} \quad (11)$$

where ε is the interaction strength, σ is the effective size of the interacting objects and Δr is their distance.

For the interaction between two spheres $\sigma = \sigma_s$ is chosen. To calculate the force on the rod i due to the rod j, Eq. (11) is used as a Kihara like potential [36] by using the shortest distance between the corresponding line segments of the rods for Δr. For nonparallel rods, this shortest distance and the corresponding vector Δr are calculated by means of the algorithm in Ref. [37]. The size σ of the rods is modeled by $\sigma = \sigma_{sc}$. By understanding the spheres as spherocylinders with line segment $l = 0$, the interaction between rods and spheres can be calculated analogously. Then, the expansion σ is chosen as $\sigma = \sigma_{eff} = (\sigma_{sc} + \sigma_s)/2$. The interaction strength is set to $\varepsilon = 1k_BT$ for all particle interactions.

Describing the collision between two particles, one can assume that the equilibrium between the total force acting on a colloid and the friction force is reached in every time step. So the usage of the overdamped approximation stays justified under particle collision and the interaction of different-shaped particles is completely captured by using σ_{eff} in the potential.

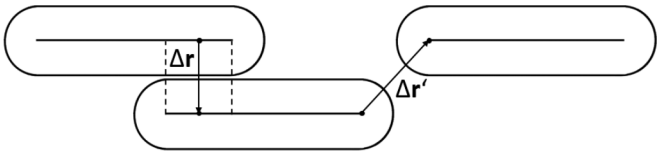

FIG. 2. Interaction of parallel spherocylinders: The left and the middle rods show the selection of Δr and the point of force application for an existing imaginary displacement perpendicular to the rod orientation resulting in an overlap of the lines. If there is no displacement causing an overlap, Δr and the point of force application will be chosen as presented by the middle and the right spherocylinder and as marked with Δr′.

Due to the nonspherical shape of the spherocylinders, the point of force application is important. In the more general case of nonparallel rods, it is assumed that it is given by the point which the shortest distance connects to the other particle of the pair interaction. For parallel spherocylinders, an additional case differentiation has to be done, whereby the approach used in this work differs from Ref. [37]. If an imaginary displacement perpendicular to the orientation of the rods which results in an overlap of the line segments does exist, the center of this overlap on the corresponding line segment is used as the point of force application. This is shown via the left and middle spherocylinder in Fig. 2. If there is no displacement which results in an overlap, the end of the line segment pointing to the other particle is used. This is presented by the interaction of the middle and the right spherocylinder in Fig. 2. In both cases, the specific points mentioned are also used as a basis to calculate the shortest distance Δr and the corresponding vector Δr for the computation of the interaction force.

An off-center force results in an additional torque M with the absolute value

$$|M| = hF \sin(\sphericalangle(\mathrm{h}, \mathrm{F})). \quad (12)$$

Consequently, the orientation of the interacting rods is affected. Here, h is the vector characterizing the lever, $h = |\mathrm{h}|$ and $F = |\mathrm{F}|$.

To compute the influence of the walls on a sphere, Δr is chosen as the vector parallel to the shortest distance Δr between the wall and the center of the regarded particle. For rods, the interaction between the wall and the spherical caps is used to calculate the resulting forces. In both cases, $\varepsilon = 10k_BT$ is used and σ is $\sigma_s/2$ for spheres and $\sigma_{sc}/2$ for rods.

Central to the following observations, a constant force **F** pointing in the x direction is applied to the spherocylinders to drag them through the bath of smaller spheres. The direction of the force can be represented with the unit vector $\hat{e}_F$. Based on the shape of the rods, a degree of freedom is given by the position $h \in [0, l/2]$ of the point of force application on the line segment measured in relation to the center of the rods. An off-center force is connected to an additional external torque affecting the orientation of the rods. In the case of absent spheres, the rotational movement of a single rod is based solely on rotational diffusion for a force applied to the center due to the decoupling of the rotation and the translation ensured by the symmetry of the spherocylinders.

The applied external driving forces used in this study are of the magnitude $F \leqslant 200 k_B T/\sigma_s$. As a consequence, the resulting velocities of the rods are limited by $v_M = 5D_s/\sigma_s$ which can be approximated by means of Eq. (7) after neglecting the noise. Therefore, the spherocylinders move less than a distance of $1.25\sigma_s$ in the time scale the overdamped two-dimensional spheres need to diffuse through an area of σ_s^2. Thereby, the time scale of sphere diffusion can be characterized in units of the Brownian time $\tau_D = \sigma_s^2/D_s$. It follows that the movement of the rods due to the driving force is still comparable to the Brownian motion of the spheres and thus the characteristic time scale for the spherocylinder drive is also of the magnitude of the Brownian time τ_D. The other relevant time scale is the Brownian relaxation time, which can be used as a crude upper bound on the colloid velocity decorrelation time [38]. Furthermore, it is used as an indicator for the negligibility of inertial terms in the Langevin description. In the following, it is assumed that the Brownian relaxation time of the rods can be roughly approximated by ten times the Brownian relaxation time $\tau_B = m_s/\zeta_s$ of the sphere. Here, m_s is the mass of the spheres and ζ_s is the friction coefficient of the spheres according to the Stokes law. In general colloid systems the Brownian relaxation time τ_B is small against the Brownian time τ_D which characterizes also the time scale in which the movement due to the driving force is relevant. This stays valid for the rods. Hence, it is reasonable to assume that inertial terms are still negligible and the description of the motion by the overdamped Langevin equation stays valid regardless of the external force.

Another aspect is that the characteristic length scale of the rods regarding the flow of the inherent bath of the Brownian dynamics algorithm differs from the one of the spheres by a factor of the magnitude of the rod length L. One can conclude that the Reynolds number of a single spherocylinder in the flow based on the application of the force F is still significantly small for the overdamped approximation regarding the rod movement to be justified.

In colloidal systems with additional external forces it is also justified to assume the fluctuation terms of the equations of motion to be Brownian, if the overdamped approximation stays valid. This corresponds to the simplification of replacing the noise by its equilibrium counterpart.

C. Observables and order parameter

To check whether the bath of spheres is in a nonequilibrium state, the mean square displacement of the colloidal spheres in flow equilibrium is observed. The equilibrium behavior of the one-dimensional mean square displacement in the x direction of the channel follows the well-known relation

$$\mathrm{MSD}(t) = 2D_{\mathrm{eff}}t \tag{13}$$

in the long-time limit, where $D_{\mathrm{eff}} \leqslant D_s$ is the diffusion coefficient for one sphere diffusing through its environment of other particles. Deviations of this law corresponding to a superdiffusive behavior are used as an indication that the spheres are driven out of equilibrium by the moving rods.

The main topic of this work is the ordering of the driven spherocylinders in the systems relative to the direction of the driving force. To analyze the mean orientation of the rods, the order parameter

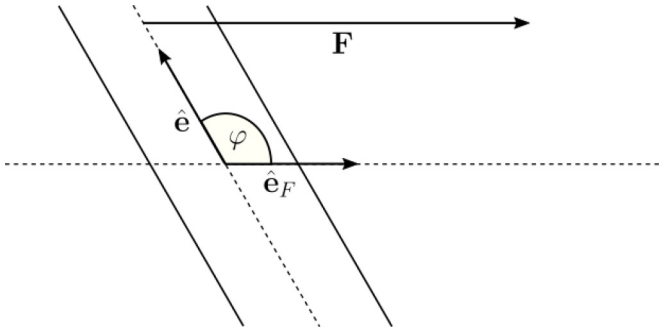

FIG. 3. A spherocylinder with the corresponding unit vector ê marking its orientation. The application point of the constant driving force F is always placed in the half of the line segment to which ê is pointing. The angle φ is defined by the angle between ê and the force direction $\hat{\mathbf{e}}_F$.

$$P_O(\tau) := 1 - 2\langle(\hat{\mathbf{e}}(t)\cdot\hat{\mathbf{e}}_F)^2\rangle \tag{14}$$

was defined, where $\tau = \frac{1}{N_t}\sum_{j=1}^{N_t} t_j$ and N_t is the number of adjacent simulation steps t_j for a mean over the time to smooth the resulting curve. Altogether, the average in Eq. (14) is given by averages over the time, the N rods in the system, and different simulations. By definition of the inner product, it is clear that the relation

$$P_O(\tau) = 1 - 2\langle\cos^2(\varphi(t))\rangle \tag{15}$$

is satisfied, where $\varphi(t) = \sphericalangle(\hat{\mathbf{e}}(t), \hat{\mathbf{e}}_F)$ is the angle between the force direction and the rod orientation. Thus, a perfect orientation parallel to the force corresponds to $P_O = -1$ and a perfect perpendicular ordering is equivalent to $P_O = 1$. A totally random orientation of the rods results in $P_O = 0$. To categorize the ordering, one can assume that $P_O < 0$ relates to a preferred mean orientation parallel to the force and $P_O > 0$ means that a mean orientation perpendicular to $\hat{\mathbf{e}}_F$ is favored. The angle φ is marked in Fig. 3.

To further describe the ordering phenomena of the spherocylinders, an examination of free energy surfaces is done. Therefore, this nonequilibrium system is compared to an effective equilibrium system with equivalent properties based on one rod in an effective mean potential W_{eff}. The influences of the external torque, the nonequilibrium environment of spheres, the wall boundary conditions, and the additional rods in the system are condensed into W_{eff} which generates the mean torque affecting the rod. This potential of mean force [39] is observed with fixed lever h as a function of the angle φ. The probability density of φ for a random orientation of the rod is given by the uniform distribution

$$p_0(\varphi) = \frac{1}{\pi}. \tag{16}$$

In a histogram with n_{bin} bins of size $\Delta\varphi = \pi/n_{\mathrm{bin}}$ the probability distribution is approximated at angles $\varphi_i = (i - 0.5)\Delta\varphi$, $i = 1, \ldots, n_{\mathrm{bin}}$ by counting the number $Q(\varphi_i)$ of observed values of $\varphi \in [\varphi_i - \frac{\Delta\varphi}{2}, \varphi_i + \frac{\Delta\varphi}{2}]$. Thus, the probability density $p(\varphi_i)$ is approximated by dividing the particular values through the total number of counts and the bin size.

The effective potential W_{eff} can be estimated by assuming a Boltzmann distribution

$$\frac{p(\varphi_i)}{p_0(\varphi_i)} \stackrel{!}{=} \exp\left(-\frac{W_{\text{eff}}(\varphi_i)}{k_B T}\right). \tag{17}$$

By using Eq. (16), one obtains the relation

$$\frac{W_{\text{eff}}(\varphi_i)}{k_B T} = -\ln\left(\frac{Q(\varphi_i)}{\Delta\varphi/\pi}\right) \tag{18}$$

for the potential of mean force.

Another observable calculated in this work is the mean velocity in force direction $\langle v_x \rangle$. This quantity is analyzed analogously to the order parameter.

D. Bridging to experimental realizations

In the following, only the above presented numerical treatment of the system is considered. Nevertheless, it is important to motivate and discuss possible experimental realizations of this complex two-dimensional system. The experimental observation of general two-dimensional (2D) colloid systems and monolayers [1,40] as well as two-dimensional channel geometries [10,11,41] is a wide field with diverse methods. To realize the two-dimensional binary mixture of spherocylinders and spheres, a monolayer of rodlike colloids mixed with smaller disks could be absorbed on a flat surface. Thereby, the rods should be absorbed in a way that they only rotate in the monolayer of colloids. A homogeneous force field like gravity in sedimentation experiments would act like a force on the center of a spherocylinder. But in experiments with optical tweezers it would in principle be possible to apply a force on a different point on the main axis of the spherocylinder. In general, the suspension of soft spheres models a complex fluid. Thus, one could expect similar ordering phenomena for the spherocylinder in specific liquids without additional disks.

As stated, hydrodynamic interactions are neglected in the following studies. However, in different experimental realizations various hydrodynamic interactions exist. These additional long range interactions become significant for the system due to the relatively high area fractions used in the system and the motion of the spherocylinders. For example, hydrodynamic interactions are found to affect the lane formation in three-dimensional sphere systems [42]. Despite this, it is reasonable to assume that the inclusion of hydrodynamic interactions modify the ordering effects discussed here but do not completely suppress them.

III. RESULTS AND DISCUSSION

All results of the Brownian dynamics simulations are given in units of the sphere diameter σ_s, the thermal energy $k_B T$, the diffusion coefficient of the spheres D_s, and the Brownian time τ_D, which is of the magnitude of the time a small sphere needs to diffuse roughly the distance of its own diameter σ_s. Only the lever arm h corresponding to the application point of the external driving force is presented in units of $l/2$ instead of σ_s.

All performed simulations consist of 8.0×10^6 simulation steps with a length of $\Delta t = 7.5 \times 10^{-5}$. The start positions and orientations are chosen randomly. During all simulations, every 800th time step is saved and used for the following analysis. For the mean over the saved steps $N_t = 625$ is chosen. The full system is based on a channel geometry with box lengths $L_x = 200$ in the x direction and $L_y = 40$ in the y direction. Altogether 40 spherocylinders are randomly placed in the resulting simulation box. So, an area fraction of $\phi_{sc} \approx 34.82\%$ results. The remaining area is filled with 2500 spheres, so that the area fraction of the spheres compared to the remaining area is $\phi_s \approx 37.65\%$. Deviations of this setup are mentioned in the corresponding sections.

It was investigated how the application point of a constant driving force which is applied to the spherocylinders influences the structures formed in the channel. In the performed simulations the point of force application is placed on a positive multiple of the orientation vector $\hat{\mathbf{e}}$, as implied in Fig. 3. This selection rule breaks the symmetry between $\varphi < \pi/2$ and $\varphi > \pi/2$ regarding the rod orientation in comparison to the force direction so that the external torque M favors an angle $\varphi = 0$.

First, the two limits of a centered force and a force applied to one end of the spherocylinders were checked. Hereby, "ends of spherocylinder" denotes the end points of the line segment, hence the maximum lever is $h = l/2$.

Figure 4(a) shows a snapshot of the system, where the force $F = 100$ in the x direction is applied to one end of the spherocylinders which corresponds to a lever $h = l/2$ taken after 5.0×10^6 simulation steps. For the full movie see Movie 1 of the Supplemental Material [43]. It can be found that this setup causes a mean orientation of the rods parallel to the force direction. Furthermore, formation of lanes can be identified, as known from pedestrians and animals moving in opposite directions [23–25,44], from analogous colloidal systems [3,18–22], and from binary plasmas [45].

Figure 4(b) shows a snapshot of the system, where the force $F = 100$ in the x direction is applied to the center of the spherocylinders. It is taken at the same simulation time as the snapshot of Fig. 4(a). For a full movie of this setup see Movie 2 of the Supplemental Material [43]. Surprisingly, in contrast to the previous process, a different ordering effect occurs. After some time, the spherocylinders order in an orientation perpendicular to the direction of the force forming long clusters. The ordering state of Fig. 4(b) is not stable in the configuration of the force of Fig. 4(a).

In Fig. 4(a) as well as in Fig. 4(b), it is apparent that the moving rods generate density fluctuations in the bath of spheres, which are a sign of its nonequilibrium character. Without the external force the spheres enter an equilibrium state but due to the external force acting on the spherocylinders the bath of spheres is constantly driven out of equilibrium while the spherocylinders enter a dynamical equilibrium.

A. Nonequilibrium state of the spheres

The nonequilibrium state of the small spheres in the case of driven rods is visible in a deviation of the equilibrium progression of the mean squared displacement in the x direction. To check the nonequilibrium behavior of the sphere bath, the mean square displacement in the x direction for $F = 0$ as well as $F = 100$ are computed, so that a direct comparison is possible.

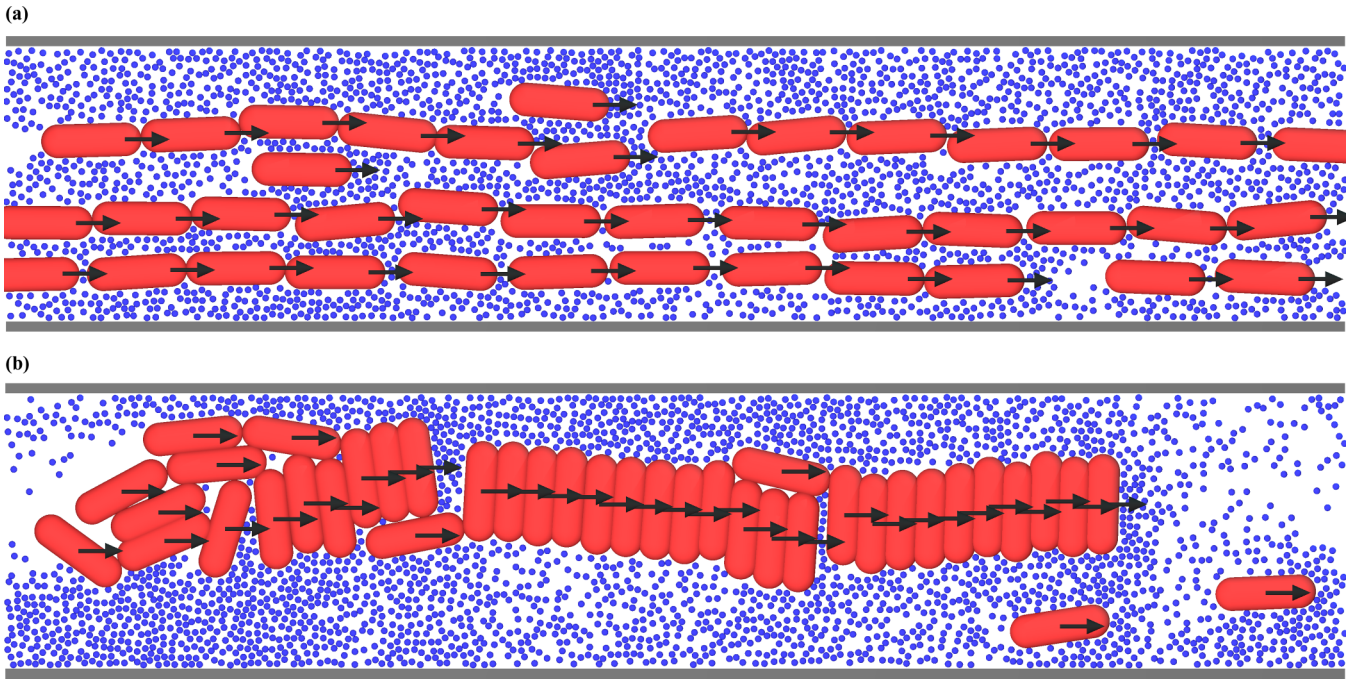

FIG. 4. Rods dragged through a bath of small spheres with a constant force $F = 100$ applied (a) either to one of their ends (see Movie 1 of the Supplemental Material [43] for the full movie) or (b) to their centers (see Movie 2 of Supplemental Material [43] for the full movie). The snapshots are taken after 5.0×10^6 simulation steps. The arrows indicate the point of application of the force and its direction. In the first case the spherocylinders order in an orientation parallel to the applied force and form lanes, whereas in the latter case the spherocylinders orient perpendicular to the applied force and form clusters.

Only the limits of a centered force and a force attached to one end of the spherocylinders is checked. However, if these two states show a nonequilibrium behavior, all lever arms between $h = 0.00$ and $h = 1.00$ will show similar results. The curves for the particular mean square displacements are plotted in Fig. 5. The results are calculated by means of an average over all spheres and ten simulations. The black line in Fig. 5 indicates the limit MSD $= t^2$ for ballistic motion with velocity $v_x = 1$.

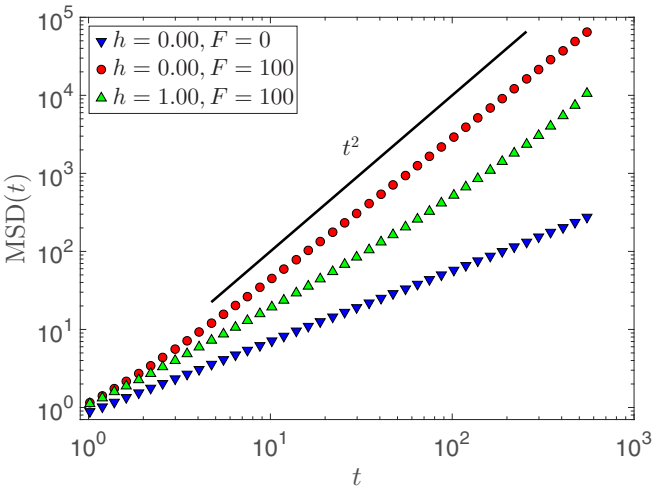

FIG. 5. Mean square displacement of the small spheres for a force $F = 100$ and the levers $h = 0.00$ and $h = 1.00$ applied to the rods in comparison with the result for rods which are not driven. The black lines shows the limit MSD $= t^2$ for ballistic motion with velocity $v_x = 1$.

For $F = 0$ the spheres can enter the thermal equilibrium and thus the mean square displacement follows the well known law given by a linear time dependency. The curves for the systems with driven rods possess higher slopes in the logarithmic plot of Fig. 5. This clearly points to a superdiffusive behavior indicating a nonequilibrium of colloidal spheres: The movement of the rods affects the bath by dragging some of the spheres along the spherocylinder trajectories. This results in a superdiffusive motion regarding the average over all particles of the bath of spheres. This phenomenon entails the density fluctuations visible in Fig. 4. In conclusion, it is safe to say that the bath of spheres is in a nonequilibrium state regarding the full accessible time window of the simulations.

B. Mean orientation of the spherocylinders

Different levers lead to different quasistatic mean orientation states of the spherocylinders. Hereby, the mean orientation of the rods shifts from a parallel to a perpendicular orientation compared to the force direction for decreasing lever arms. In the following, this behavior is analyzed with the defined order parameter.

A constant driving force $F = 100$ is applied in the x direction on the spherocylinders. The orientational ordering due to the constant driving force is an effect that occurs in a flow equilibrium. From a random starting position the system needs some time to reach this flow equilibrium.

Figure 6(a) shows the time dependency of the order parameter (14) for different levers $h \in \{0.00, 0.10, 0.20, 0.30,$

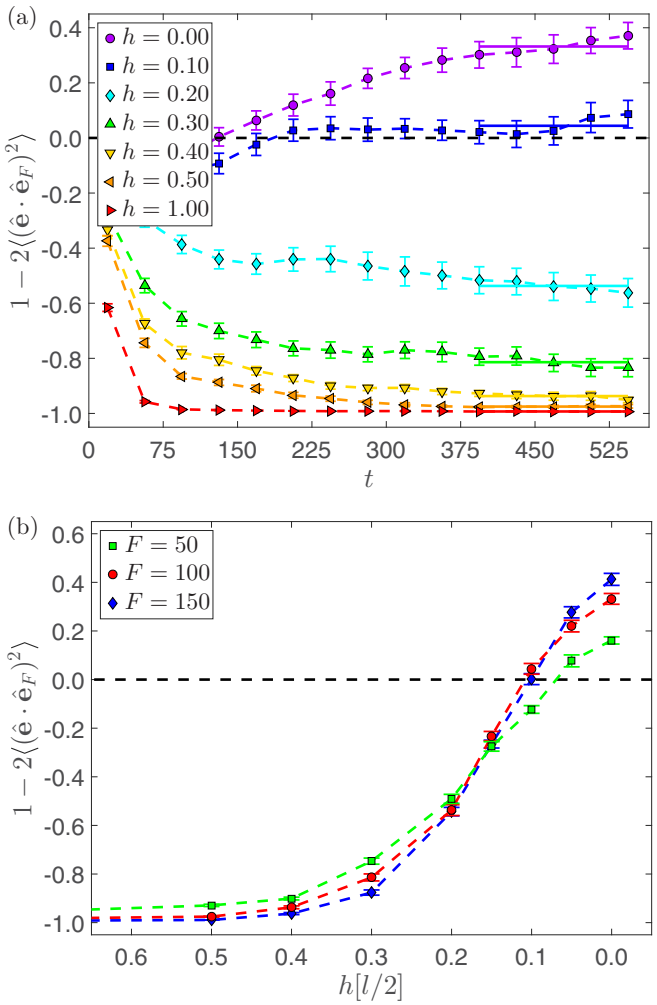

FIG. 6. (a) Time evolution of the order parameter for $F = 100$ and different levers. A negative order parameter corresponds to an orientation parallel to the driving force and a positive value corresponds to an orientation orthogonal to the force. The value for a random orientation is marked with a black dashed line. The last five points of every curve are used to calculate the final state order parameter. (b) The approximated final state value of the order parameter as a function of the lever for different forces $F \in \{50, 100, 150\}$. The random orientation P_O is marked with a dashed black line.

0.40, 0.50, 1.00}. All values are averaged over 20 simulations with different random starting positions. The uncertainty of the order parameter is estimated by the standard deviation of the mean value for the average over all simulations. The value for a completely random orientation is $P_O = 0.00$. It is marked with the black dashed line.

For long levers, the order parameter converges to a value near $P_O = -1.00$ and thus to an orientation parallel to the force. In a sufficient approximation, quasistatic values between $P_O = -1.00$ and $P_O = 0.00$ can be found regarding the accessible time window by reducing the lever arm. Hereby, the corresponding end values are increased for shorter lever arms. For the centered force, the order parameter rises distinctly over the value of random orientation. On average an orientation perpendicular to the force is favored for $h = 0.00$. The resulting order parameter for $h = 0.10$ is also slightly above the value for random orientation.

It should be noted that the curves in Fig. 6(a) do not reach a perfectly static end value in the observed time window: The results for long levers still show a small downward trend and the curves for short levers seem to possess an upwards tendency. For example, the last points of the curve of $h = 0.00$ seem to indicate that the order parameter starts to rise again for higher times. Similar results are present for other, larger forces. However, in the following, it is assumed that the order parameters reached a quasistatic final state regarding the observed time window in a sufficient approximation. This assumption ensures a comparison between the different levers which corresponds to the used maximum number of simulation steps. Because the curves for long levers show a small downward trend and the curves for short levers show a small upward trend, the observed separation in two distinct ordering states would only become more obvious for more simulation steps and thus the utilized assumption can easily be justified: The qualitative results of the following analysis would only become more apparent for a larger time interval. Further simulations with more simulation steps may lead to different final state values for short levers like $h = 0.00$. For long levers the calculated finale state values most certainly match the corresponding flow equilibrium values of the long-time limit.

In conclusion, the final state value of the order parameter rises with a decreasing lever arm. A force applied near the center of the rods results in a preferred orientation of the rods perpendicular to the direction of the applied force.

An approximation for the flow equilibrium order parameter depending on the lever arm can be calculated with the results of the time evolution. Therefore, an average of the last five points of every curve in Fig. 6(a) is taken as an estimate for the final state value regarding the observed time window. Its uncertainty is estimated with error propagation. The calculated final state values serve a mostly qualitative analysis of the observed phenomenon and its lever dependency. Thus, the choice of five points for the average is a sufficient approximation for the end values regarding the accessible simulation time. The resulting values can be plotted over the lever arm h. The final state order parameter is calculated for the seven levers used in the analysis of the time dependency as well as the additional levers $h \in \{0.05, 0.15\}$.

The corresponding curve is plotted in Fig. 6(b) and in Fig. 8(a) with red circles. With decreasing lever arms the mean orientation of the rods shifts from a parallel to orthogonal orientation compared to the direction of the applied force, whereby the process starts in a region of $h = 0.50$. The resulting curve intersects the line for random orientation between $h = 0.15$ and $h = 0.10$, around which we define the critical lever for a transition between phases ordered parallel and perpendicular with respect to the applied force.

It is reasonable to assume that the mean orientation of the rods depends on the strength of the external force. Thus, for each force $F \in \{50, 100, 150\}$ the order parameter is plotted as a function of the lever arm h in Fig. 6(b). For these three forces the order parameter for $h = 0.00$ reaches approximately its flow equilibrium value regarding the time window of the simulation.

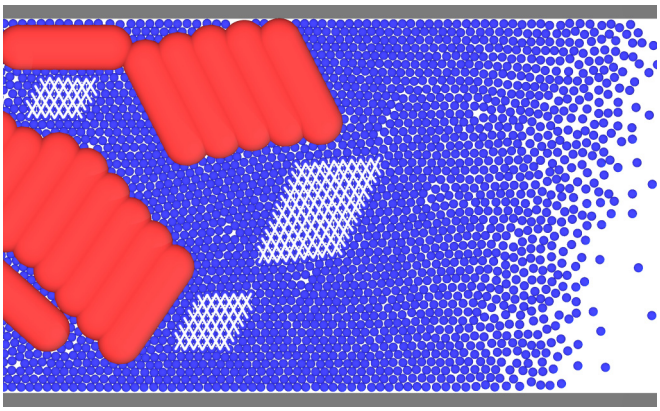

FIG. 7. Crystal of spheres formed due to the density enhancement in the front area of the spherocylinder structures for $F = 200$ and $h = 0.00$. The resulting triangular lattice is marked with white lines in some areas of the crystal.

All order parameter curves of the different forces intersect roughly in a range between $h = 0.20$ and $h = 0.05$. With this one can identify three distinct regions regarding the observed forces: long lever arms ($h > 0.20$) with parallel orientation, intermediate levers ($0.05 < h \leqslant 0.20$) with mixed orientation clearly dominated by a favored parallel orientation, and short lever arms ($h \leqslant 0.05$) with mixed orientation mostly dominated by an orientation orthogonal to the force.

As shown in Fig. 6(b), the values of the order parameter are higher for smaller forces in the range of longer lever arms $h > 0.20$. This is a reasonable result, since the external torque, which aligns the spherocylinders parallel to the force, decreases by weakening the applied force. For smaller forces the orientational fluctuations become more and more dominant and hinder the perfect parallel orientation. In the domain of short levers given by $h \leqslant 0.05$, the ordering orthogonal to the force direction is strengthened by increasing the force and thus the maximum of the order parameter at $h = 0.00$ increases with higher absolute values of the force. An important result is that the found transition between the two ordering states is clearly visible for all analyzed forces.

Simulations with higher forces like $F = 200$ showed an additional interesting phenomenon affecting the order parameter especially clearly: A temporary crystallization of the bath of spheres. By dragging the spherocylinders through the surrounding system, bow waves of spheres are created. These waves cause high density fluctuations in the environment of the rods based on the spheres. This effect is especially dominant for short lever arms and thus most notably for $h = 0.00$. The local density around the front area of the ordered rod structures are primarily increased. The strength of this density enhancement grows with the absolute value of the applied force. For high forces the density is increased so much that even crystallites of the solely repulsive spheres can form. This effect is shown in Fig. 7 for $F = 200$. To enhance the visibility, the resulting triangular lattice is marked with white lines for some areas of the crystal.

Rods surrounded by the two-dimensional sphere crystal orient along the crystal planes. From the perspective of the dynamics of the system, the resulting crystal appears to be a stronger obstacle of the spherocylinders. So they reorient due to the interaction with it. Due to alignment effects of the crystal planes parallel to the channel walls, an orientation of the spherocylinders perpendicular to the driving force is hindered, and thus order parameter values can become smaller compared to the values in a system with slightly smaller driving forces (like $F = 150$). In general, the formed sphere crystals are not stable regarding the full simulation time. Thus, in the long-time limit the dissolution of the crystals allowed short lever final state order parameters of $F = 200$ to climb above the corresponding values of lower forces. Similar crystallization phenomena occur for all analyzed forces in a lesser extent.

C. Influence of the specific system parts

The simulation setup based on the channel and the binary colloid mixture represents a highly complex system. So the particular parts of the setup influence the outcome of the ordering processes in different ways. By selectively removing and re-adding parts of the system, we found that the observed ordering phenomenon appears mostly due to the small spheres and the usage of multiple rods.

To gain a better understanding of the observed phenomenon, it is necessary to remove crucial elements of the simulation setup and compare the different results. Therefore, we check different area fractions, systems with and without small spheres, and the influence of the channel walls.

We start with systems without small spheres, to see which effects can already be seen in a system of spherocylinders dispersed in a simple liquid. The first system consists of a box characterized through $L_x = 200$ and $L_y = 500$, periodic boundary conditions, and $N = 40$ spherocylinders without any spheres. The resulting area fraction of the rods, $\phi_{sc} \approx 2.79\%$, is so low that interactions are negligible. Thus, the ordering behavior due to the rotational Brownian motion can be observed adequately enough without losing the statistic based on the number of rods. The result averaged over 50 simulations is marked with blue downward-pointing triangles in Fig. 8(a). For $h \geqslant 0.10$ the rods order mainly parallel to the force because of the external torque caused by the off-center driving force. In the range of $h \leqslant 0.05$, the external torque is smaller than the rotational diffusion. Thus, the order parameter rises to the value of random orientation $P_O = 0.00$ marked with a black dashed line. At the lever arm $h = 0.00$, the final state order parameter reaches the value for random orientation. In general, the progression of the order parameter in this system can be explained by the ratio of the aligning torque and the rotational diffusion alone.

The next step is to increase the number of the spherocylinders to $N = 500$, while still omitting the small spheres. By this means, the area fraction of rods $\phi_{sc} \approx 34.82\%$ is similar to the one of the full system. With this setup the influence of the enhanced interaction probability due to the higher area fraction is investigated. Due to the higher number of spherocylinders the results were only averaged over 20 simulations. In Fig. 8(a) the resulting curve is marked with green upward-pointing triangles. For this system the order parameter already starts to rise between $h = 0.15$ and $h = 0.10$, so that the corresponding curve progresses above the

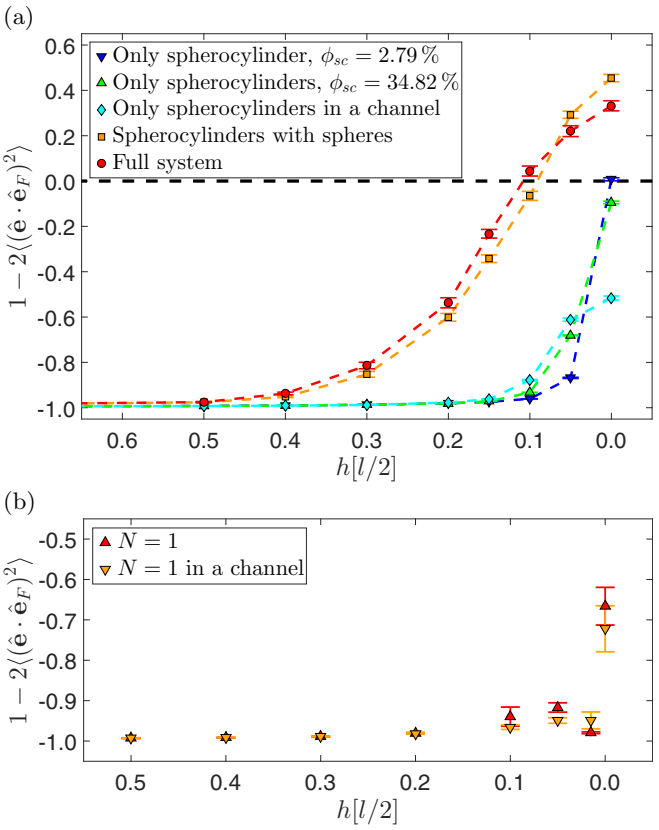

FIG. 8. (a) The final state order parameter as a function of the lever arm for different combinations of the system parts and $F = 100$. The value for random orientation is marked with a black dashed line. The two upper curves originate from systems with small spheres. Thereby, the curve marked with orange squares is based on a rod-sphere mixture without a channel geometry. The three lower curves originate from systems without small spheres. In both cases the channel walls reduce the order parameter for $h \to 0$. (b) The final state order parameter as a function of the lever for a single rod in the bath of spheres. The values for the lever arm $h = 0.00$ are clearly below the value for random orientation $P_O = 0.00$.

result for $\phi_{sc} \approx 2.79\%$. Moreover, the order parameter for a force acting on the center at $h = 0.00$ is lowered compared to the previous result. Overall, the enhanced area fraction reduces the orientation parallel to the force a little bit for short levers. But a preferred orientation perpendicular to the applied force is not reached solely due to the enhanced interaction probability.

To study the influence of the restriction caused by the channel walls, 50 simulations of only spherocylinders in a channel are conducted. $N = 40$ spherocylinders are used. The results are depicted with cyan diamonds in Fig. 8(a). In this system the order parameter is strongly reduced for small levers because of the channel geometry. Only a value of $P_O(0.00) = -0.52(1)$ is reached, since the channel boundary conditions enforce an orientation parallel to the force, because the rods align parallel to the walls while approaching them.

By re-adding the spheres into the system and changing the channel boundary conditions into periodic ones, the curve marked with orange squares in Fig. 8(a) is an average over 20 simulations with a box based on $L_x = 200$ and $L_y = 40$. A preferred orientation perpendicular to the force is achieved. The final state order parameters for the levers $h = 0.00$ and $h = 0.05$ are clearly above the random value and the order parameter rises already in the region of $h = 0.50$. Consequently, the bath of spheres is crucial to the observed perpendicular ordering mechanisms.

By comparing the results for periodic boundary conditions with spheres and the results of the full system, one obtains a similar relation as through the comparison of the curve for periodic boundary conditions without spheres and the channel geometry without spheres: The channel results in a reduction of the order parameter for short lever arms.

Another crucial element of the system is the many-body character of the spherocylinder system. Thus, the mean orientation of a single rod in the bath of spheres is observed to see the difference in orientation compared to a system with multiple rods. Therefore, the length of the box is rearranged to save simulation time. The new simulation parameters are given by $L_x = 125$ and $L_y = 40$. 2350 spheres were used, so that the area fraction compared to the rest area is $\phi_s \approx 37.44\%$. Simulations for periodic boundary conditions and a channel geometry are conducted. The results are presented in Fig. 8(b).

The values for the lever arm $h = 0.00$ of both curves are close to the value $P_O(0.00) \approx -0.70$. This value is clearly below the value for random orientation. So the spherocylinder orients parallel to the force and without the other rods in the system a mean orientation parallel to the force results.

To summarize, the bath of small spheres has opposite effects on the orientation of a single spherocylinder and of multiple interacting spherocylinders if the force is applied near the center. A single spherocylinder in a bath of small spheres prefers an orientation parallel to the force instead of a random orientation, whereas multiple interacting spherocylinders in a bath of small spheres prefer an orientation perpendicular to the force.

What is the mechanism in systems of multiple rods in a bath of spheres that leads to the formation of clusters of rods with an orientation perpendicular to the force direction in the case of short lever arms? As visible in movies of the simulations (see Movie 2 of the Supplemental Material [43]) this is a nonequilibrium many-body phenomenon, that has its origin in the enhanced clustering due to the different velocities in the channel direction of the particular spherocylinders.

Rods which are by chance orientated orthogonal to the force direction move slower than rods with a parallel orientation to the force direction. This comes already from the lower diffusion coefficient orthogonal to the main axis of the spherocylinder $D^{\perp}$, but is strongly enhanced by the influence of the spheres facing the rods in the force direction. Thus, orthogonal oriented slower spherocylinders are caught up by faster moving spherocylinders. This effect is further enhanced by the additional velocity difference due to the sphere slipstream created by the slower spherocylinders (and already existing clusters) which benefits the rods catching up. This results in a rapid formation of big clusters. Thereby, the particular spherocylinders of a cluster are aligned by interactions with the surrounding particles and additional spherocylinders which also catch up to the cluster.

Once these clusters are formed, an orientation perpendicular to the force direction is the most stable state for them.

For example, if the individual rods of the cluster are oriented parallel to the force, the cluster is easily destroyed due to velocity fluctuations. In contrast, if the spherocylinders of the cluster are oriented perpendicular to the force direction, the lifetime of the cluster is considerably enhanced. Moreover, the influence of the sphere flow on the cluster becomes symmetrical if they form an angle $\varphi = \pi/2$ with respect to the flow. The bath of spheres should also enhance the lifetime of the particular rod clusters in the system analogously to the well known enhanced clustering due to entropic depletion forces in colloidal equilibrium systems [46] with depletion agents.

In conclusion, the bath of spheres and high enough area fractions of the spherocylinders are both crucial for the observation of the transition between the different mean orientations.

D. Distribution functions and potential of mean force

According to the previous section, the different parts of the systems alter the results for the order parameter in various ways so that a detailed description of the full system is highly complex. However, some information regarding transition between the two observed ordering effects is contained in the probability densities $p(\varphi)$ for different levers.

In the following, the distribution of the orientation of the spherocylinders in the flow equilibrium and a description based on a potential of mean force of a virtual equilibrium system are used to further visualize the transition between two different ordering states.

For this analysis we used the results of the force $F = 150$, which showed the maximum effect. Figure 9(a) shows an analysis of the angular distributions by calculating a normalized φ histogram with a bin size of $\Delta\varphi = \pi/25$ by means of the data of 20 simulations. For this, the orientations of the rods were computed every 800 steps after the threshold step 3.2×10^6 is passed. As a reference curve for random orientation the uniform probability density is marked with the black dashed line. The levers $h \in \{0.00, 0.10, 0.20, 0.30\}$ are analyzed.

For $h \in \{0.10, 0.20, 0.30\}$, the probability for values of φ lower than $\varphi \approx \pi/6$ is increased compared to the random orientation. Only for $h = 0.00$, one gets a contrary result for this range. The resulting values near $\varphi = \pi/2$ are enhanced for $h \in \{0.00, 0.10\}$. The curve of $h = 0.30$ is distinctly lowered for mid- and high-range values of φ.

By using the numerically computed distributions of the orientations for $F = 150$ shown in Fig. 9(a), the potential of mean force W_{eff} of a corresponding equilibrium system with the same angle distribution can be calculated by means of Eq. (18). The resulting free energy surfaces are displayed in Fig. 9(b). To enhance clarity, the particular curves are shifted by steps of $4k_BT$. The marked black lines correspond to the relative zero levels.

For $h > 0.10$, a dominant minimum can be found for $\varphi = 0$. Due to the external torque, the effective potential proceeds below the relative zero level. Passing a region of $\varphi = \pi/6$, the effective potential is enhanced for higher values of φ. Figure 9(b) shows that this dominant minimum diminishes for decreasing lever arms. On the other hand, an additional minimum is formed near $\varphi = \pi/2$. For $h = 0.00$, the minimum at $\varphi = 0$ is nearly completely above the zero level and the second minimum is clearly dominant. The discrepancy between the angles for the second minimum regarding $h = 0.00$ and $h = 0.10$ is a result of the external torque, in general shifting the orientation to lower angles. This can be seen in the probability densities as well. The first minimum corresponds to the orientation parallel to the force direction and the second minimum near $\varphi = \pi/2$ is connected with the orientation perpendicular to the applied force, so the vanishing dominance of the minimum at $\varphi = 0$ and the formation of

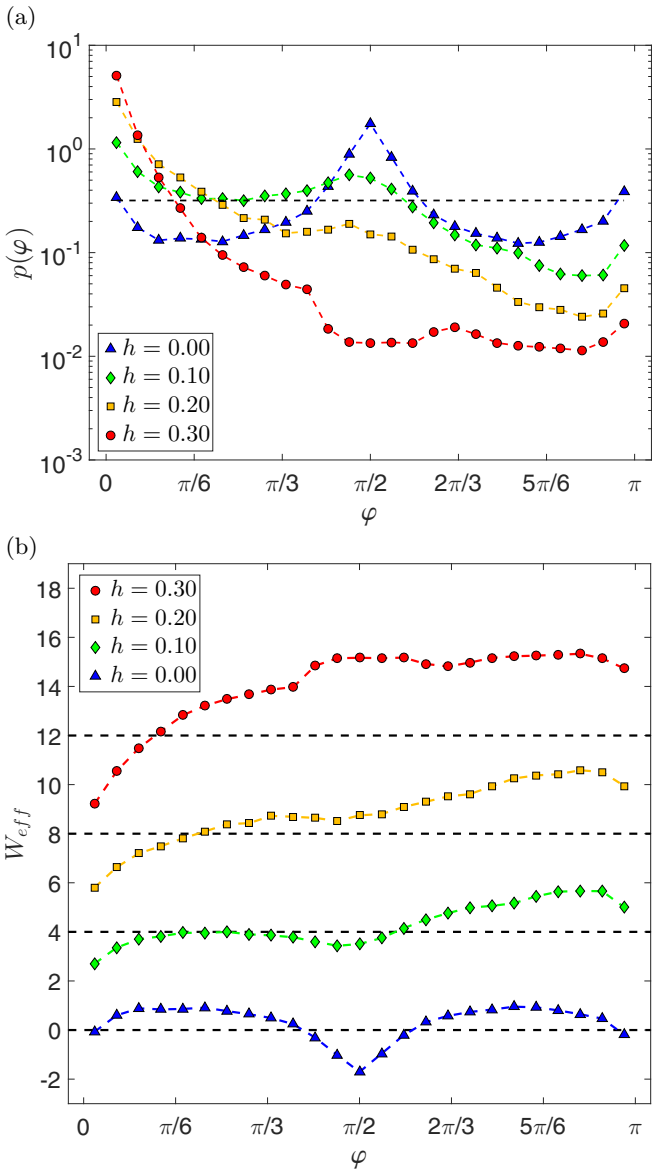

FIG. 9. (a) The probability density $p(\varphi)$ of the orientation angle φ for a driving force of $F = 150$ and for different lever arms after a final state is reached, in a histogram with bin size of $\Delta\varphi = \pi/25$. The black dashed line indicates the uniform angular distribution of free spherocylinders. (b) Potential of mean force for the final state in dependency of the angle φ for a driving force of $F = 150$ and for different lever arms. The particular curves are shifted in steps of $4k_BT$. At $\varphi = 0$, a minimum can be found which diminishes for decreasing lever arms. On the other hand, a second minimum is formed near $\varphi = \pi/2$.

the second minimum near $\varphi = \pi/2$ for decreasing lever arms is a clear indication for a transition between two phases. For $h = 0.00$, the resulting effective potential exhibits a symmetry where the second minimum near $\varphi = \pi/2$ acts as symmetry center. In Figure 9(b) it is visible that this symmetry is broken by shifting the point of force application from the center to one end of the spherocylinders. Hence, an increasing lever results in a tilt of the effective potential to lower values of φ and a vanishing of the minimum near $\varphi = \pi/2$. It should be mentioned that the tilt of the curves caused by the external torque is a result of the broken symmetry due to the numerical selection rule regarding the positioning of the point of force application on the different halves of the line segments.

By observing the progression of the potentials of mean forces in Fig. 9(b), it seems as if the formation of the second minimum for decreasing lever arms starts not at the angle where the first minimum is located. This discrepancy between the angles corresponding to the first minimum and the formation of the second minimum indicates that the transition between the two observed phases of orientation can be described by a first order phase transition [47] (for equilibrium systems in the thermodynamic limit). This is backed by the coexistence of both phases which can be found in Fig. 4(b).

E. Flow equilibrium mean velocity

Another interesting observable is the mean velocity of the spherocylinders in the channel direction because it is directly linked to the orientation of the rods. For different levers the mean velocity also reaches different quasistatic final values. The progression of these values regarding the lever further confirms the transition between two orientation states.

To analyze the mean velocity, the data of the simulations with $F = 100$ are used. The results of these calculations are presented in Fig. 10(a). The uncertainties are estimated with the standard deviation of the mean value for the average regarding the different simulations.

For all lever arms h it can be noticed that the mean velocity first increases until it fluctuates around a constant value of the flow equilibrium. Looking at levers $h > 0.20$, this final state velocity increases for longer levers. In contrast, this clear ordering is not true for short levers. Here the resulting value for $h = 0.00$ is above the results of $h = 0.10$ and $h = 0.20$. Even for a centered force an enhancement of the particle velocity over time can be observed. With this one can argue that the ordering reduces internal friction between the spherocylinders and the bath of small spheres.

The results depicted in Fig. 10(a) imply that the flow equilibrium behavior of the mean velocity can be controlled by the lever arm. Therefore, the transport properties of the colloid system in the channel could be adjusted by changing the point of force application.

To analyze the lever dependency, a procedure similar to the calculation of the final state order parameter is chosen. As marked in Fig. 10(a), the average of the last five points of every curve is taken. The resulting values are plotted over the lever arm h in Fig. 10(b). In this case the uncertainties are estimated by error propagation.

In general, the resulting functional progression of the final state mean velocity in dependency of the lever can be approximated by an s-shaped curve typically marking the transition between two distinct states. The first state is given by the low mean velocity values of the curve depicted in Fig. 10(b), which correspond to the previously discussed mean orientation perpendicular to the force. After the value $h = 0.15$ is reached, a lengthening of the lever arm entails a rise of the final state mean velocity. For long levers the slope of the curve declines until the second state is reached. This state is connected with a mean orientation parallel to the force. For short levers $h \leqslant 0.15$ the resulting final state velocities are close together and a clear trend of the final state mean velocity in this region is not apparent.

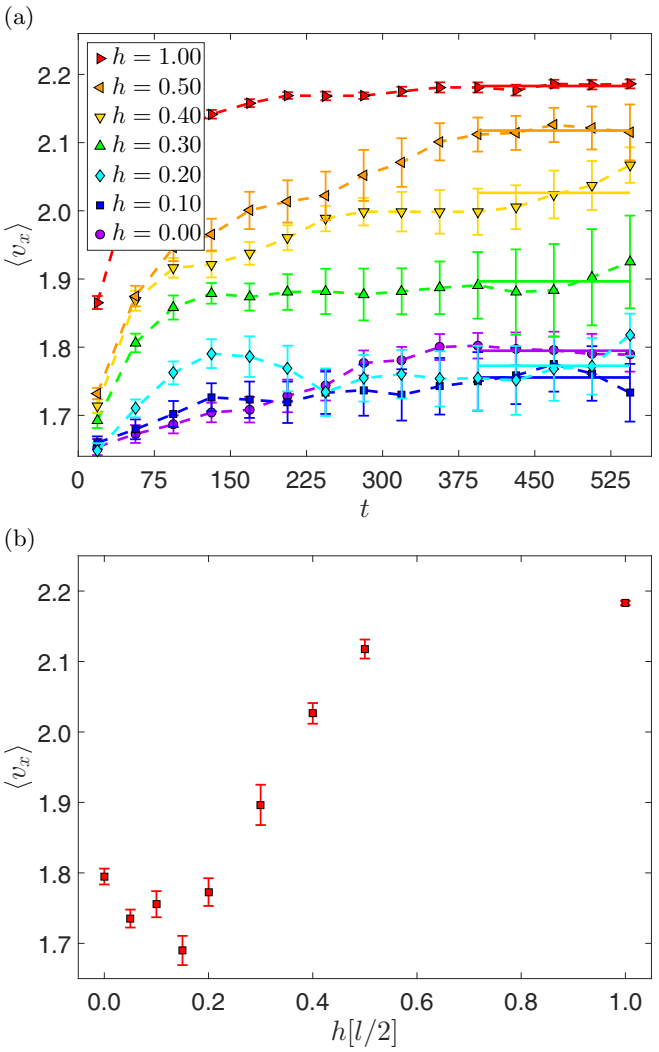

FIG. 10. (a) Time evolution of the mean velocity for $F = 100$ and different levers. The curves converge to a flow equilibrium value. The mean of the last five points of every curve is used to calculate the final state velocity. (b) Final state mean velocity in dependency of the lever arm h. The functional progression results in an s-shaped curve.

F. Finite size analysis and critical lever

To check the influence of finite size effects on the observed ordering transition, a finite size analysis was conducted. The results of this analysis suggest that the observed ordering

transition of the rods seems to be a general phenomenon of the rod-sphere mixture and independent of the chosen size of the channel geometry. However, the absolute values of the final state order parameters can vary for different setups. Only for too small channel lengths L_x, nonphysical finite size effects suppress the transition.

First, we define the critical lever as the lever h_c for which $P_O(h_c) = 0$. This specific quantity marks the transition between the range of favored parallel orientation with $P_O < 0$ and the range with a preferred orientation perpendicular to the force characterized by $P_O > 0$. This is the quantity of interest.

Two different studies are performed: First, the effect of the general size of the system on the ordering transition is observed by scaling the area of the simulation box by varying L_x and L_y while the ratio L_y/L_x is kept constant. In total the areas $L_xL_y \in \{1600, 2000, 2666.67, 4000, 8000, 16\,000\}$ are checked. The second study analyzes the influence of the periodic boundary conditions by varying the channel length L_x for two different channel widths $L_y \in \{30, 40\}$. Here, simulations for the lengths $L_x \in \{40, 50, 66.67, 100, 200, 400\}$ are performed. For both studies and all observed systems the area fractions of rods and spheres are kept constant.

To calculate a first approximation of the critical lever, the final state order parameters for the levers $h \in \{0.08, 0.10, 0.12\}$ are calculated analogously to the previous sections. The two consecutive values h_1, h_2 with $P_O(h_1) > 0$ and $P_O(h_2) < 0$ of the levers $h \in \{0.08, 0.10, 0.12\}$ are used to calculate a straight line. Then, the zero crossing of this line is used as an approximation for h_c. If there is not a consecutive pair of the observed levers which marks a conversion of the final state order parameter, simulations with additional levers are conducted. The errors of the calculated h_c are approximated with maximal error estimation by using the various straight lines which result from all possible combinations of the mean values and corresponding error interval limits. Hereby, lines with a zero crossing not in the range between $h = 0.00$ and $h = 0.15$ are neglected: All performed simulations showed that the final state order parameter of $h = 0.15$ is clearly below zero.

Due to the low particle number of rods in the small systems, the resulting order parameters fluctuate strongly. So, a transition of the ordered states and thus the critical lever is only accepted, if there is at least one additional lever $h \in \{0.00, 0.04, 0.08, 0.10\}$ with an order parameter value $P_O(h) > 0.10$.

The results of the first study are depicted in Fig. 11(a). The approximations of the critical lever arms of all observed areas are within good agreement with each other. Thus, one can assume that the ordering transition is a phenomenon of the sphere-rod mixture and not of the dimensions of the simulation box. Even small simulation setups showed the transition between the two ordering phases. However, it should be noted that the absolute vales of final state order parameters for short levers vary for the different areas. The average of particular values for the different areas is presented with the dashed line in Fig. 11(a). It is of the magnitude of $h_c \approx 0.11$.

Figure 11(b) shows the results of the second study. The small systems with $L_x \in \{40, 50\}$ do not show the ordering transition so the corresponding values are absent in Fig. 11(b).

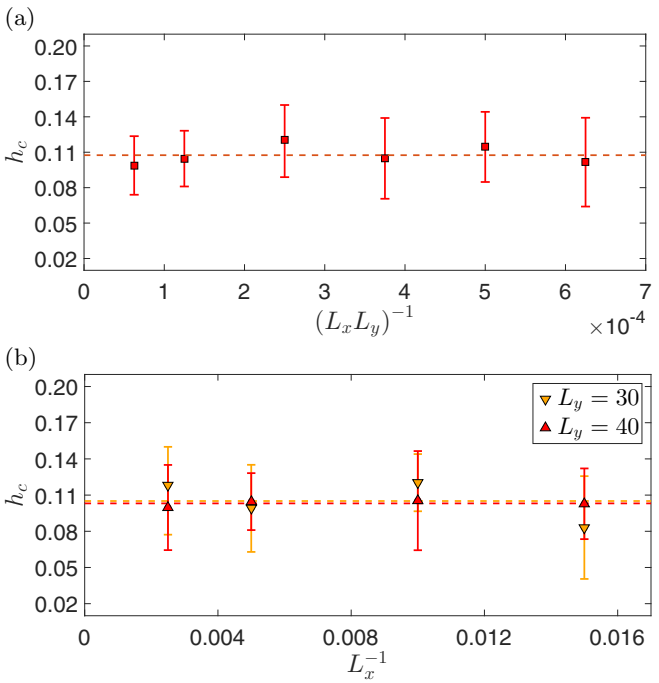

FIG. 11. (a) Critical lever h_c in dependency of the inverse of the area of the simulation box, whereby the ratio L_y/L_x is kept constant for the different observed areas. The dashed line shows the average regarding the particular points. (b) Critical lever h_c in dependency of the inverse length of the channel geometry for two different channel widths. The dashed lines show the averages which correspond to the resulting points of the particular widths.

For these simulation setups, finite size effects seems to matter: The system is likely to form structures with lengths as long as the channel in front of one of the channel walls. Due to the periodicity of the simulation box, these structures move through the channel without interacting with spheres in their direction of motion. This is valid for both channel widths.

The critical levers of the different channel lengths are comparable with the results of the first study. Therefore, one can assume that finite size effects regarding the periodic boundary conditions do not affect the ordering transition in a dominant way for systems with acceptable channel lengths. The averages of the resulting points of the particular widths are marked with dashed lines in Fig. 11(b). The average of $L_x = 30$ is of the magnitude of $h_c \approx 0.11$ and the average of $L_x = 40$ is of the magnitude of $h_c \approx 0.10$.

In conclusion, the finite size studies indicate that the ordering phenomena of the observed system are independent of the absolute area for $L_y/L_x = \text{const.}$ and of the used channel length for sufficient L_x. Thus, it seems that a change of preferred orientation is a general phenomenon of the rod-sphere mixture. By means of the studies, the critical lever of the chosen parameters is around $h_c \approx 0.11\,l/2$. By using the definition of the line segment and $\sigma_{sc} = 5\sigma_s$, it shows that the critical lever is of the magnitude of $\sigma_s/2$. However, it should be noted that the critical lever depends on the used diffusion coefficients of the spherocylinders and thus it differs for other parameters.

IV. CONCLUSION

The detailed study of nonequilibrium systems leads to interesting phenomena that are a central topic of modern research. The aim of this work was to analyze the ordering phenomena of driven spherocylinders in a suspension of smaller spheres embedded in a two-dimensional channel geometry. Therefore, an order parameter was defined and analyzed after the nonequilibrium character of the bath of spheres was confirmed by an observation of the mean square displacement.

By means of numerically computed probability distributions, an analysis of the potential of mean force for an equivalent equilibrium system was possible. The dynamic ordering of the rods is linked to the mean velocity in the channel direction. Thus, this observable was numerically calculated and discussed.

The main finding is a transition from a preferred orientation parallel to the force direction to a preferred orientation perpendicular to the force when shortening the lever arm. Furthermore, a force dependency was found for this transition. An analysis of potentials of mean force showed a diminishing minimum for the orientation parallel to the force and the formation of a minimum for the orientation perpendicular to the force further indicating the transition between two phases. This transition is also backed by the results for the lever dependency of the final state mean velocity. To increase the understanding of the observed highly complex colloid system, crucial parts of the systems were removed and combined in different variations. This led to the result that the small spheres and the many-body character of the rod system are necessary to find a mean orientation perpendicular to the applied force at short levers. In simulations of a single spherocylinder in the bath of spheres the favored state is a mean orientation parallel to the force.

The results of a finite size study indicates that the ordering transition is a general phenomenon of the observed rod-sphere mixture. The performed studies allude to a critical lever of the magnitude of $h_c \approx 0.11\, l/2$, where l is the length of the spherocylinder line segment.

The presented results show the interesting nature of the observed complex nonequilibrium system. In further studies it would be interesting to observe the system in the limit of large simulation time values and to investigate the parameter behavior focused on different aspect ratios, spherocylinder diameters, and forces. Furthermore, a detailed analysis analogous to Ref. [48] could bring a deeper understanding of the collective behavior of the rod clusters for short levers. Regarding the critical lever, further simulations with different ratios of σ_{sc} and σ_s could lead to a better understanding of the critical quantities and thus to a deeper insight of the whole system.

ACKNOWLEDGMENTS

The authors gratefully acknowledge the SFB 1214 for support, and the Gauss Centre for Supercomputing e.V. (Ref. [49]) for funding this project by providing computing time through the John von Neumann Institute for Computing (NIC) on the GCS Supercomputer JUWELS at Jülich Supercomputing Centre (JSC).

[1] T. Bohlein, J. Mikhael, and C. Bechinger, Nat. Mater. **11**, 126 (2012).
[2] U. Siems and P. Nielaba, Phys. Rev. E **91**, 022313 (2015).
[3] B. Heinze, U. Siems, and P. Nielaba, Phys. Rev. E **92**, 012323 (2015).
[4] S. R. Nagel, Rev. Mod. Phys. **89**, 025002 (2017).
[5] J. Berner, B. Müller, J. Gomez-Solano, M. Krüger, and C. Bechinger, Nat. Commun. **9**, 999 (2018).
[6] T. Brazda, A. Silva, N. Manini, A. Vanossi, R. Guerra, E. Tosatti, and C. Bechinger, Phys. Rev. X **8**, 011050 (2018).
[7] J. M. Pagès, A. V. Straube, P. Tierno, J. Ignés-Mullol, and F. Sagués, Soft Matter **15**, 312 (2019).
[8] J. Olarte-Plata, J. M. Rubi, and F. Bresme, Phys. Rev. E **97**, 052607 (2018).
[9] R. Haghgooie and P. S. Doyle, Phys. Rev. E **70**, 061408 (2004).
[10] P. Henseler, A. Erbe, M. Köppl, P. Leiderer, and P. Nielaba, Phys. Rev. E **81**, 041402 (2010).
[11] U. Siems, C. Kreuter, A. Erbe, N. Schwierz, S. Sengupta, P. Leiderer, and P. Nielaba, Sci. Rep. **2**, 1015 (2012).
[12] D. Wilms, N. B. Wilding, and K. Binder, Phys. Rev. E **85**, 056703 (2012).
[13] U. Siems and P. Nielaba, Phys. Rev. E **98**, 032127 (2018).
[14] M. Dreher, F. Pauly, J. Heurich, J. C. Cuevas, E. Scheer, and P. Nielaba, Phys. Rev. B **72**, 075435 (2005).
[15] F. Pauly, J. K. Viljas, M. Bürkle, M. Dreher, P. Nielaba, and J. C. Cuevas, Phys. Rev. B **84**, 195420 (2011).
[16] T. M. Squires and S. R. Quake, Rev. Mod. Phys. **77**, 977 (2005).
[17] B. Zhang and M. Radisic, Lab Chip **17**, 2395 (2017).
[18] J. Dzubiella, G. P. Hoffmann, and H. Löwen, Phys. Rev. E **65**, 021402 (2002).
[19] T. Glanz and H. Löwen, J. Phys.: Condens. Matter **24**, 464114 (2012).
[20] T. Vissers, A. Wysocki, M. Rex, H. Löwen, C. P. Royall, A. Imhof, and A. van Blaaderen, Soft Matter **7**, 2352 (2011).
[21] K. Ikeda and K. Kim, J. Phys. Soc. Jpn. **86**, 044004 (2017).
[22] C. Reichhardt, J. Thibault, S. Papanikolaou, and C. J. O. Reichhardt, Phys. Rev. E **98**, 022603 (2018).
[23] D. Helbing, L. Buzna, A. Johansson, and T. Werner, Transp. Sci. **39**, 1 (2005).
[24] M. Moussaïd, D. Helbing, and G. Theraulaz, Proc. Natl. Acad. Sci. USA **108**, 6884 (2011).
[25] J. Lee, T. Kim, J.-H. Chung, and J. Kim, KSCE. J. Civ. Eng. **20**, 1099 (2016).
[26] G. A. Vliegenthart and H. N. W. Lekkerkerker, J. Chem. Phys. **111**, 4153 (1999).
[27] A. V. Kyrylyuk, A. Wouterse, and A. P. Philipse, AIP Conf. Proc **1145**, 211 (2009).
[28] R. Kirchhoff and H. Löwen, J. Phys.: Condens. Matter **17**, 7805 (2005).
[29] H. E. Bakker, S. Dussi, B. L. Droste, T. H. Besseling, C. L. Kennedy, E. I. Wiegant, B. Liu, A. Imhof, M. Dijkstra, and A. van Blaaderen, Soft Matter **12**, 9238 (2016).
[30] M. Grünwald, S. Tricard, G. M. Whitesides, and P. L. Geissler, Soft Matter **12**, 1517 (2016).

[31] H. Löwen, H. H. Wensink, and M. Rex, AIP Conf. Proc **982**, 284 (2008).
[32] D. L. Ermak, J. Chem. Phys. **62**, 4189 (1975).
[33] H. Löwen, Phys. Rev. E **50**, 1232 (1994).
[34] M. M. Tirado and J. G. de la Torre, J. Chem. Phys. **81**, 2047 (1984).
[35] J. D. Weeks, D. Chandler, and H. C. Andersen, J. Chem. Phys. **54**, 5237 (1971).
[36] T. Kihara, Rev. Mod. Phys. **25**, 831 (1953).
[37] C. Vega and S. Lago, Comput. Chem. **18**, 55 (1994).
[38] J. T. Padding and A. A. Louis, Phys. Rev. E **74**, 031402 (2006).
[39] J. G. Kirkwood, J. Chem. Phys. **3**, 300 (1935).
[40] F. Ebert, P. Dillmann, G. Maret, and P. Keim, Rev. Sci. Instrum. **80**, 083902 (2009).
[41] R. Haghgooie, C. Li, and P. S. Doyle, Langmuir **22**, 3601 (2006).
[42] M. Rex and H. Löwen, Eur. Phys. J. E **26**, 143 (2008).
[43] See Supplemental Material at http://link.aps.org/supplemental/10.1103/PhysRevE.99.022601 for movies of the different ordering effects due to a constant external force $F = 100$ applied either to the centers of the spherocylinders or to one of their ends. The movies show the progression of the system during 5.0×10^6 simulation steps.
[44] I. D. Couzin and N. R. Franks, Proc. R. Soc. London, Ser. B **270**, 139 (2003).
[45] K. R. Sütterlin, A. Wysocki, A. V. Ivlev, C. Räth, H. M. Thomas, M. Rubin-Zuzic, W. J. Goedheer, V. E. Fortov, A. M. Lipaev, V. I. Molotkov, O. F. Petrov, G. E. Morfill, and H. Löwen, Phys. Rev. Lett. **102**, 085003 (2009).
[46] T. Biben, P. Bladon, and D. Frenkel, J. Phys.: Condens. Matter **8**, 10799 (1996).
[47] K. Binder, Rep. Prog. Phys. **50**, 783 (1987).
[48] N. C. X. Stuhlmüller, T. Eckert, D. de las Heras, and M. Schmidt, Phys. Rev. Lett. **121**, 098002 (2018).
[49] www.gauss-centre.eu.